Contrib Mineral Petrol (2000) 139: 163–179

Ronald J. Bakker · Manish A. Mamtani

Fluid inclusions as metamorphic process indicators in the Southern Aravalli Mountain Belt (India)

Received: 24 March 1999 / Accepted: 13 January 2000

Abstract Fluid inclusions from a biotite-garnet schist in the Southern Aravalli Mountain Belt (India) give information on both peak metamorphic conditions and post-peak metamorphic processes during uplift. A combination of careful petrography, microthermometry and Raman spectroscopy reveals the presence of at least five generations of enclosed fluids. Lower amphibolite-facies pressure-temperature conditions of the growth of garnet rims are reproduced by the highest fluid density of the relatively oldest inclusion type of CO_2 ($\pm N_2$)-rich compositions. A calculated fluid composition in the COH system, in equilibrium with the graphite buffer corresponds to a CO_2-rich fluid at metamorphic conditions. However, the results of these calculations are very sensitive to small fluctuations in oxygen fugacity and the accuracy of thermodynamic properties of mineral equilibria. Re-equilibration, conceived by specific size-density distribution and the absence of an aqueous phase in inclusions that contain nahcolite crystals, is monitored in these inclusions as post-peak metamorphic processes, like partial decrepitation and preferential leakage. The other fluid types represent heterogeneous fluid trapping of coexisting aqueous NaCl-bearing solutions with CO_2-CH_4-rich vapour bubbles in healed cracks, and probably the introduction of external fluids containing high salinity aqueous $CaCl_2$-rich solutions in nearly pure N_2 vapour bubbles, at lower *P-T* conditions. This study illustrates that fluid inclusions remain a valuable database of peak metamorphic conditions, moreover, alterations of the entrapped fluids and surrounding crystals are illustrative for specific exhumation evolutions.

R. J. Bakker (✉)[1]
Geologisch-Paläontologisches Institut,
Universität Heidelberg, INF 234, D-69120 Heidelberg, Germany

M. A. Mamtani[2]
Department of Geology,
M.S. University of Baroda,
Vadodara, 390002, India

Present addresses:
[1]Institut für Geowissensehatten,
Mineralogie und Petrologie, Montan-Universität,
A-8700 Leoben, Austria
E-mail: bakker@unileoben.ac.at

[2]Department of Geology and Geophysics,
Indian Institute of Technology,
Kharagpur-721302, West Bengal, India
E-mail: mamtani@gg.iitkgp.ernet.in

Editorial responsibility: J. Touret

Introduction

A study of fluid inclusions can provide vital information about the fluids that were present during metamorphism and hence the thermal history of the rock, which can supplement geothermobarometric studies, carried out by other independent techniques (e.g. microprobe studies). The application of fluid inclusions as geothermometers and geobarometers for metamorphic rocks has been considered since Sorby (1858), who described a general decrease in degree of filling (vol.% of liquid H_2O) of fluid inclusions in quartz in schist towards granite stocks in Cornwall. The importance of fluid inclusion studies in metamorphic rocks was reinforced by e.g. Touret (1977). However, the reliability of fluid inclusions as paleo-environment indicators has been taken as questionable in metamorphic rocks. Lamb et al. (1987) argued about the existence of CO_2-rich fluids during peak metamorphic conditions in granulites, and concluded a post-metamorphic origin of fluid inclusion based on oxygen-fugacity calculations from mineral equilibria and the presence of graphite. Küster and Stöckhert (1997) anticipated that quartz crystals are unable to preserve original metamorphic fluids in fluid inclusions that have been entrapped at temperatures above 300 °C. Post-entrapment changes of fluid inclusions are believed to be a major argument against the application of inclusions in metamorphic studies. Decrepitation, stretching processes, and diffusion of fluid components

through crystals have been experimentally studied by e.g. Bodnar et al. (1989), Sterner and Bodnar (1989), Bakker and Jansen (1994), and Vityk and Bodnar (1995), and it has been suggested that these processes could also be induced in natural rocks (Hollister 1990; Bakker and Jansen 1993). In addition, complete recrystallisation of grains containing fluid inclusions can always wipe out any traces left of the original fluids and post-entrapment processes.

The aim of this study is to illustrate that metamorphic minerals are able to preserve the original metamorphic fluids in fluid inclusions. Moreover, those inclusions that have changed bulk composition and density properties may identify specific re-equilibration mechanisms and post-peak metamorphic processes that only occur at certain conditions. Although re-equilibration processes are not yet fully understood, a large variety of fluids may occur in certain inclusion assemblages because these processes do not take place uniformly within single crystals. Fluid inclusions in metamorphic rocks (lower amphibolite facies) from the Southern Aravalli Mountain Belt (SAMB), India, have been used to show that metamorphic rocks are able to preserve this geological information.

Geology of studied area

The Southern Aravalli Mountain Belt (SAMB) forms the southern fringe of the Aravalli Mountain Belt (AMB), the latter being a major Proterozoic fold belt of northwestern India. The AMB extends for a distance of around 600 km in northwestern India (Fig. 1). Lithostratigraphically, the oldest sequence in the AMB is the Archean basement referred to as the Banded Gneissic Complex (BGC, Heron 1953) or the Mewar Gneissic complex (Roy and Kröner 1996) which is a composite group of gneisses of diverse ages (Gopalan et al. 1990; Tobisch et al. 1994; Roy and Kröner 1996). These Archean basement rocks are overlain by two main Proterozoic metasedimentary and metaigneous sequences – the Aravalli (2500–2000 Ma) and the Delhi Supergroups (2000–740 Ma) (Gupta et al. 1980, 1992). The rocks presently investigated belong to the Lunavada Group (Fig. 2). It comprises an alternating sequence of quartzites and schists, occasionally with bands of calcsilicates and is the second youngest group of the Aravalli Supergroup. The Lunavada Group is overlain by the Champaner Group. It is intruded by the Godhra Granite which has been dated as 955 Ma old (Gopalan et al. 1979). The Lunavada and Champaner Groups along with the Godhra Granite comprise the SAMB.

Detailed structural studies on rocks of the Lunavada Group occupying an area of approximately 900 square km around the towns of Lunavada and Santrampur have revealed that the rocks have undergone polyphase deformation. On the basis of field studies, structural analysis and Anisotropy of Magnetic Susceptibility (AMS) studies, three episodes of deformation (D1, D2 and D3) have been recorded (Mamtani 1998; Mamtani et al. 1998, 1999a, 2000). Deformations D1 and D2 were coaxial and resulted in NE–SW trending folds. Deformation D3 resulted in WNW–ESE to E–W trending folds. The superposition of these three fold events has resulted in the development of different types of regional scale interference patterns in the Lunavada region.

Petrographic studies have revealed that metamorphism progressed up to lower amphibolite facies. Moreover, a study of several thin sections of metapelites from the entire area has revealed that the grade of metamorphism increases from the northern parts of the study area (around the towns of Ditwas and Kadana in Fig. 2) to the southern parts (south of the towns of Lunavada and Santrampur in Fig. 2). The northern, central and southern parts of the Lunavada–Santrampur area consist of chlorite schists, biotite schist and garnet-biotite schist, respectively. This implies that the southern parts of the study area represent a deeper crustal level, which has been tilted and uplifted during its evolutionary history (Mamtani et al. 1998). Microprobe measurements of garnet-biotite schist and related geothermobarometric calculations indicate that the growth of garnet from core to rim was associated with decompression (Mamtani 1998; Mamtani et al. 1999b). Moreover, porphyroblast-matrix relations using garnet and biotite porphyroblasts in garnet-biotite schists reveal that the garnet porphyroblasts have grown syntectonically with D2 deformation (Mamtani and Karanth 1997). This implies that uplift of the Lunavada orogen initiated with garnet growth during D2 deformation (Mamtani et al. 1999b).

Methods and techniques applied

A microscopic examination of doubly polished thick sections (~150 μm thickness) of the garnet-biotite schist from the Lunavada region of the SAMB (Fig. 2) was carried out. Only fluid inclusions present in quartz crystals in the schist could be investigated in detail. Although the biotite, garnet and quartz inclusions in garnet also show fluid inclusions, they were too small for microthermometric treatment. A detailed description of petrography and distribution of fluid inclusions is presented which is followed by a presentation of the results from microthermometric measurements and Raman spectroscopy. The fluid inclusions were firstly classified, based on inclusion morphologies and distribution. Microthermometric measurements were made with the Linkam stage (THM 600). The stage was calibrated using synthetic fluid inclusions of pure H_2O and CO_2-H_2O mixtures for the melting temperatures of H_2O at 0 °C, of CO_2 at −56.6 °C, and of clathrate Q2 melting at 9.9 °C. Small single grains of the pure chemical substance Phenanthrene ($C_{14}H_{10}$) were placed on the sample holder and used to calibrate at its melting temperature of 99.2 °C in the presence of a liquid rim. The samples were first subjected to rapid freezing to measure the approximate nucleation temperatures (*Tn*) of fluid inclusions. Freezing could be achieved up to temperatures of −180 °C. The samples were slowly heated to a maximum of +40 °C and temperatures of melting (*Tm*) and temperatures of homogenisation (*Th*) of fluid inclusions were recorded. Total homogenisation of aqueous inclusions has not been measured, instead volume fraction estimates were made of the phases present at room temperatures. It must be kept in mind that heating experiments can often lead to decrepitation of the inclusions and, therefore, loss of important information about the composition of the gases comprising the inclusions, especially for high density carbonic fluid inclusions. The term "carbonic" is used for CO_2-rich mixtures with varying amounts of N_2 and CH_4. In some aqueous inclusions melting of clathrate phase could be observed using the cycling method of heating and freezing on the Linkam stage. From the clearly depressed melting temperature of CO_2 in carbonic inclusions, which indicates the presence of other gases like N_2 and CH_4 it was found essential to carry out Raman spectroscopical analysis. The analyses were made with a Dilor Microdil-28 multichannel laser Raman microspectrometer using a 514 nm Ar-ion laser as source of excitation at the Free University, Amsterdam. The instrument and the measurement conditions for fluid inclusions have been described by Burke & Lustenhouwer (1987) and by Burke (1994).

Data obtained from microthermometry, Raman microspectrometry and occasionally volume fraction estimates of the fluid inclusions were evaluated by using several newly designed computer program packages *CLATHRATES* (Bakker 1997) and *FLUIDS* (Bakker 1999) in order to transform melting temperatures, homogenisation temperatures and optical volume fraction estimates into bulk compositions and densities, which are used for isochore calculations. Recently published highly accurate thermodynamic models of fluid properties, e.g. equations of state are

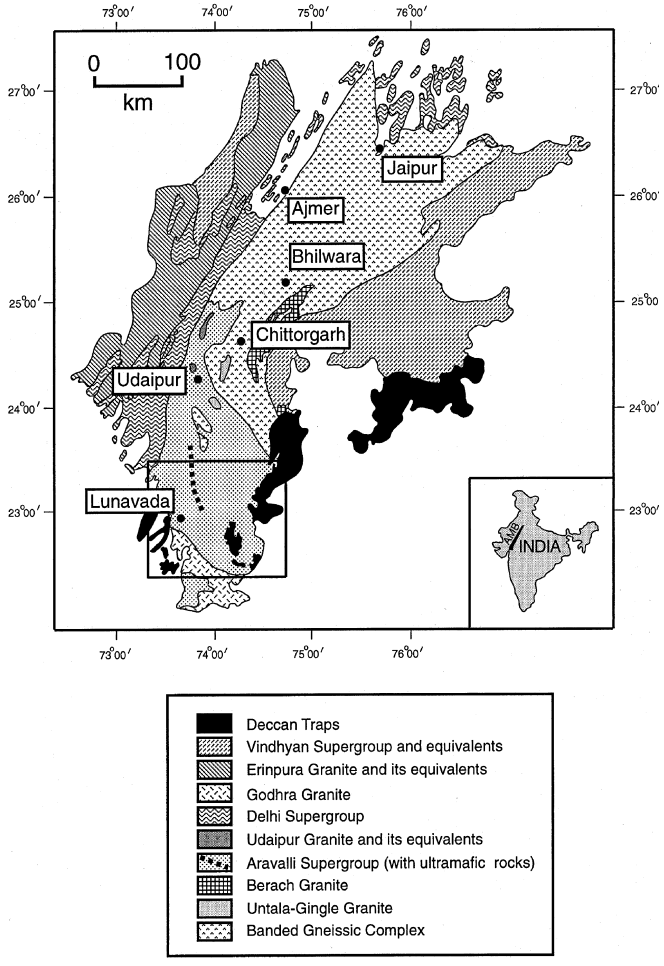

Fig. 1 Generalised geological map of the Aravalli Mountain Belt. The *box* in the southern part marks the Southern Aravalli Mountain Belt (SAMB)

incorporated in these programs. Homogenisation temperatures of carbonic CO_2-CH_4-N_2 mixtures are transformed into densities according to the modified Soave equation of state from Thiéry et al. (1994), using Lee and Kesler (1975) for volumetric properties. Pure CO_2 fluid properties are calculated with the equation of state from Duschek et al. (1990) and Span and Wagner (1996). Isochores of the entrapped fluids are traced to high temperatures and pressures, including the thermal expansion and compressibility of the host mineral quartz (Hosieni et al. 1985).

Results

Petrography of thick section

The schist investigated shows garnet and biotite porphyroblasts in the presence of a mica and quartz-rich matrix. Figure 3 is a schematic sketch of the thick section, which was investigated for the present study. The garnet porphyroblasts have a size ranging from 0.4 to 1.7 mm and preserve the schistosity (S1) in the form of quartz inclusion trails. In most garnets observed in the thin sections of this sample, the quartz inclusion trails lie at a high angle to the matrix foliation (S2). This foliation is constituted of biotite, muscovite and quartz, and a few crystals of ilmenite. The quartz crystals in the matrix show a sharp extinction and preserve 120° triple points. This quartz contains several types of solid inclusions, including apatite and clear inclusion-free single crystals (20–200 μm) coated by several euhedral graphite crystals (1–3 μm), which are probably relicts of high pressure quartz polymorphs. Furthermore, the matrix quartz has numerous fluid inclusions in different configurations, mainly in trails, along (sub-)grain boundaries and as isolated groups within the grains.

Fluid inclusion microthermometry, Raman spectroscopy and morphology

The distribution and orientation of fluid inclusions are schematically indicated in Fig. 3. Five types of fluid inclusion can be classified from inclusion morphology and distribution, in combination with microthermometric measurements and Raman spectroscopy.

Type 1 fluid inclusions

The inclusions belonging to this category comprise relatively large (15–4 μm diameter) generally equidimensional single phase inclusions (at room temperature) which occur as isolated clusters within quartz grains. Their shape varies from spherical to cylindrical and some of them also show perfect negative crystal shapes (Fig. 4a, b). At room temperature, some inclusions contain a birefringent mineral (Fig. 5a, b), which is identified with Raman spectroscopy to be nahcolite-$NaHCO_3$ (Fig. 5c). The solid/fluid ratio varies widely among neighbouring inclusions, and some of these enclosed crystals may exceed the diameter of the fluid inclusions (Fig. 5b). Graphite can be identified by Raman spectroscopy in some inclusions, appearing as a small broad peak at about 1350 cm^{-1}, interfering with the CO_2 spectrum.

Microthermometric measurements have shown that the nucleation of solid carbonic phase occurs around −100 °C. Final melting ranges between −61 and −56 °C (Fig. 6b, Table 1). These inclusions are interpreted as CO_2-rich fluids and the depression of the melting temperature of pure CO_2 implies the presence of other gases. Raman analysis (Table 4 and Fig. 7) reveals a composition of 72–96 mol% CO_2, 4–26 mol% N_2 and minor amounts of CH_4 (1–4 mol%). Homogenisation occurs generally into the liquid phase over a broad temperature interval between −45.9 and +21.6 °C (Fig. 6a, Table 1). This implies a relatively large range of densities for type 1 fluid inclusions. Only a few inclusions homogenise in the vapour phase between +22.8 and −38.9 °C. Most inclusions homogenise in the liquid phase between −16 and +12 °C (Fig. 6a) with a peak frequency at about 0 °C. To illustrate the relation between the size of these inclusions and homogenisation temperatures, the aver-

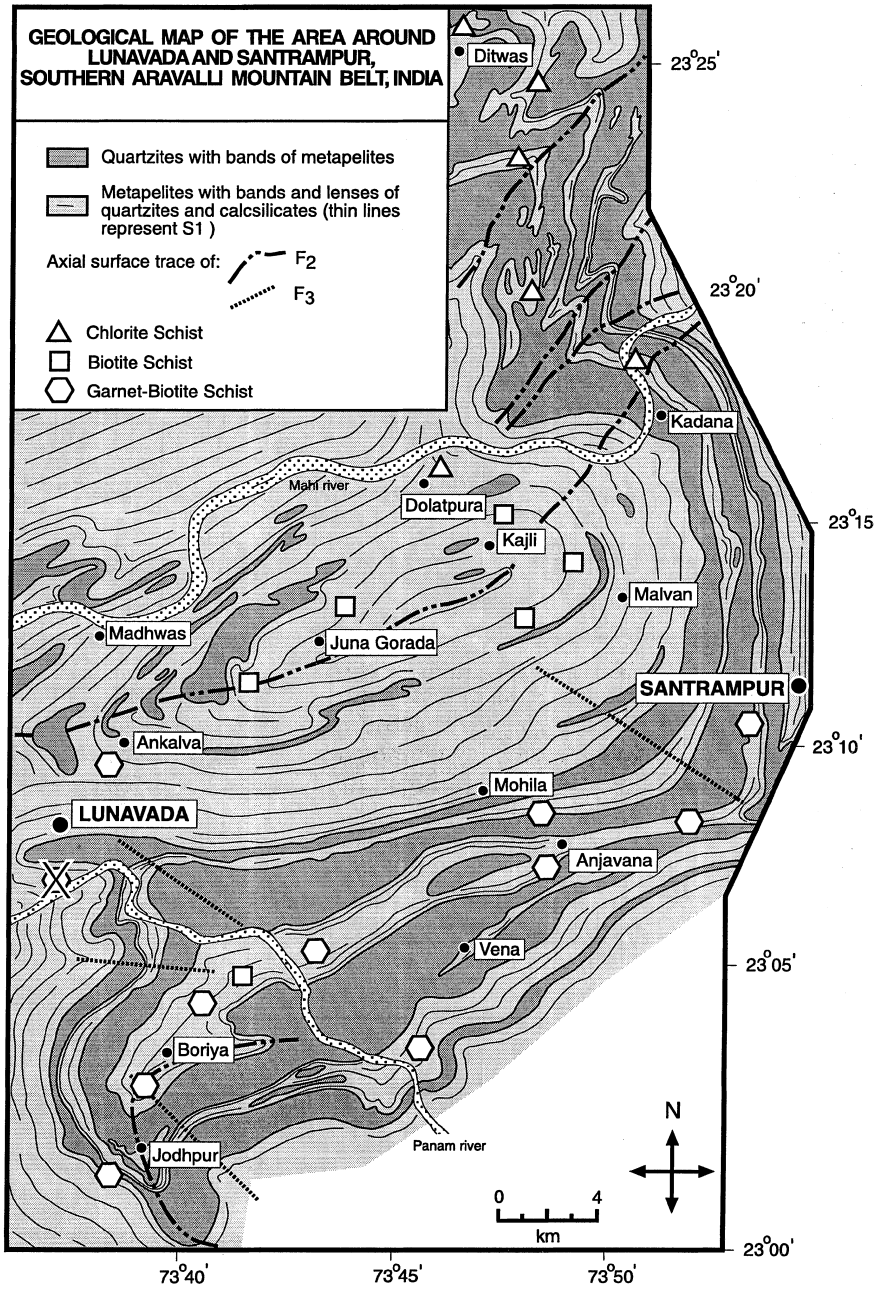

Fig. 2 Geological map of the study area. The map also shows the distribution of schists of various metamorphic grades. The sample location is marked with the *X*

age diameter of each inclusion was recorded (Fig. 8, Table 1). The trend in Fig. 8 suggests a systematic relation between *Th* and average diameter. Smaller fluid inclusions tend to have lower minimum *Th* and consequently higher densities than larger inclusions, whereas all sizes of inclusions show relatively higher *Th*, between +10 and +20 °C.

Type 2 fluid inclusions

The inclusions belonging to this class constitute trails of small fluid inclusions (< 2 μm diameter), which are also occasionally associated with bigger equidimensional dark fluid inclusions (around 13 μm diameter). The inclusion trails reveal only one pronounced orientation and lie almost perpendicular to the S2 schistosity and, therefore, also at an angle to trails of type 3 fluid inclusions (Fig. 3). The small inclusions contain two phase aqueous-rich fluids, with high filling degrees (75–95 vol.%). Relatively low melting temperatures are recorded for the aqueous solution, between −9.3 and −23.4 °C (Table 2), and eutectic temperatures lie between −50.3 and −44.7 °C. Therefore, it is assumed that $CaCl_2$ is the type of salt that predominates in this aqueous solution. Salinities are calculated to vary between 13.4 and 23.3 eq.wt% $CaCl_2$. The bigger inclusions contain a single phase fluid, that does not show any response on freezing down to −165 °C. Only

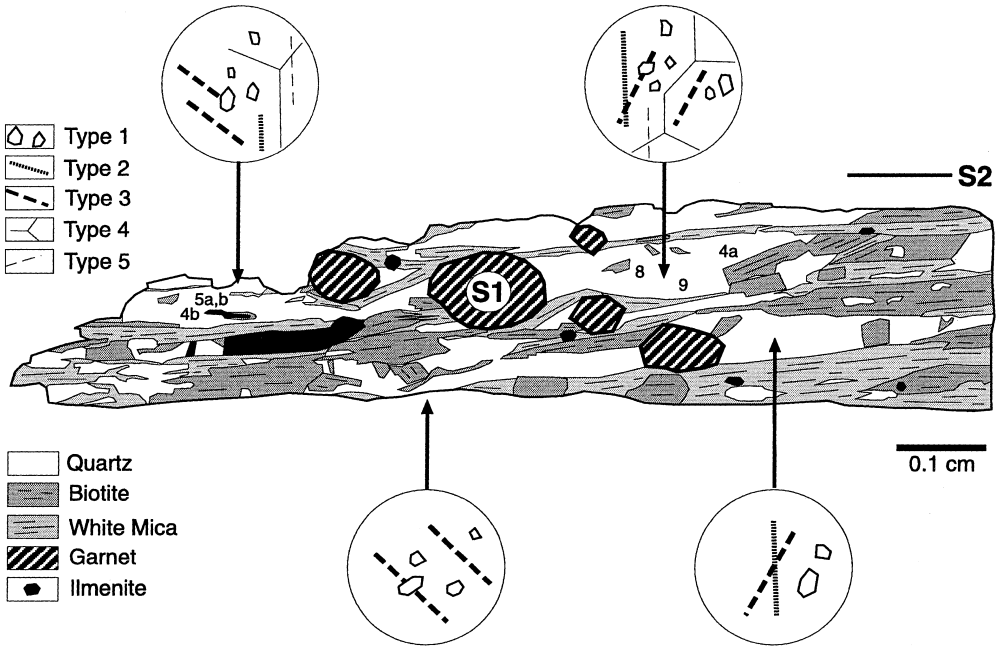

Fig. 3 Schematical drawing of the studied thick section of approximately 150 μm thickness. The occurrence of five types of fluid inclusions is schematically illustrated. The *numbers* refer to the actual position of the inclusions presented in the corresponding photomicrographs

in one inclusion a homogenisation temperature of −148 °C into the vapour phase could be measured (Table 2) which illustrates that the carbonic phase must be rich in either CH_4 or N_2 and that it has a relatively low density. Raman analysis (Table 4 and Fig. 7) shows the presence of a N_2-rich fluid (~100–92 mol%) with minor amounts of CH_4 (~0–4 mol%) and CO_2 (~0–5 mol%). On the basis of these observations it is concluded that type 2 inclusions consist of two coexisting fluids, i.e. a very low density N_2-rich fluid in association with highly saline aqueous fluids. Intermediate types of fluids are not observed.

Raman analysis has also revealed the presence of nahcolite crystals in some of the dark big fluid inclusions, furthermore, a broad graphite peak is observed at about 1352 cm^{-1}. The inclusions walls are probably coated with a thin layer of graphite, causing the dark appearance of these inclusions. It is hypothesised that these inclusions may represent pre-existing type 1 fluid inclusions which opened during fracturing and subsequently got refilled by latter fluids.

Type 3 fluid inclusion

The inclusions belonging to this class are morphologically regular shaped, equidimensional and they are in general too small (< 1 μm diameter) for microthermometric analyses, e.g. the trails in Fig. 4b. Occasionally, these trails include clusters of larger fluid inclusions (up to 15 μm diameter), which are assumed to be refilled type 1 inclusions. The inclusions dominantly comprise two phases at room temperature, i.e. liquid and vapour bubbles of variable size.

Figure 9 is a schematic drawing illustrating type 3 inclusions along these trails. The S2 schistosity is parallel to the long axis of Fig. 9 and the inclusion trail lies oblique to the S2 as well as to the field of view. A few of these inclusion trails lie oblique to each other, which probably represent conjugate sets. Aqueous inclusions show a filling degree of about 80 to 90 volume% and a few also show a moving bubble at room temperature. Such inclusions have a regular shape, usually like a cube. These inclusions occur together with usually bigger and more irregular shaped inclusions with a lower degree of filling (10–20 vol.%). Some of these inclusions clearly show an aqueous rim. They tend to have a very low density carbonic vapour phase. Such inclusions did not show any changes during microthermometric measurements. Intermediate type of fluid inclusions are also present and reveal filling degrees between 40 and 80 volume%.

Microthermometric measurements reveal that these inclusions are composed of mixed fluids. Melting temperature of the CO_2-rich phase, clathrates and the aqueous phase are measured (Table 3). Melting temperatures of ice in aqueous inclusions range between −2.3 to −6.1 °C (Table 3). Eutectic temperatures were measured in only a few inclusions and these range between −20 and −25 °C, which indicates that NaCl predominates in the aqueous solution. Subsequently, the relatively low salinity of these fluids was calculated to vary between 3.9 and 8.9 eq.wt% NaCl. Such inclusions can be considered to form the first end-member of this group (inclusions A in Fig. 9 and Table 3). The second end-member comprises richly carbonic fluid inclusions with only a rim of water (inclusion C in Fig. 9 and Table 3). The melting temperature of the CO_2-rich phase was measured between −56.3 and −61.2 °C for some inclusions (Table 3), illustrating the presence of other gases. Raman analysis (Table 4 and Fig. 7) illustrates a highly variable composition of 0 to 86 mol% CO_2 and 14 to 100 mol% CH_4

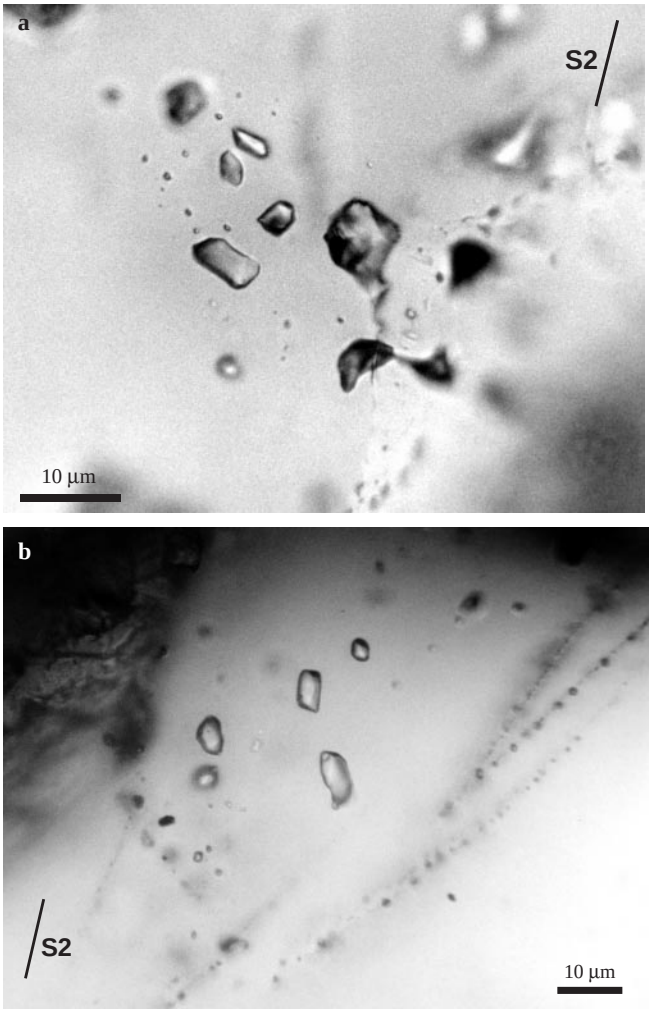

Fig. 4 Photomicrographs of type 1 fluid inclusions as isolated clusters (**a**) and in relation to trails of type 3 fluid inclusions (**b**). The orientation of the schistosity S2 is schematically illustrated

and only minor amounts of N_2. The relatively broad Raman-peak around the CH_4 position suggests the presence of other hydrocarbons in these inclusions. Only low to very low densities could be inferred from homogenisation temperatures for such vapour-like fluids. The intermediate type of fluid (inclusion B in Fig. 9 and Table 3) is characterised by the possibility to measure clathrate melting temperatures in the presence of a vapour-rich carbonic phase and an aqueous solution. These temperatures vary between $+6.8$ and $+10.2$ °C.

Type 4 fluid inclusions

Inclusions occurring along grain boundaries and subgrain boundaries of the quartz crystals belong to this category (Fig. 10). They are irregular shaped inclusions with an average diameter < 2 µm. Some of them are worm shaped, irregular voids and dendritical channels which are typical of grain boundaries. No microthermometry could be done on these inclusions on account of their minute size.

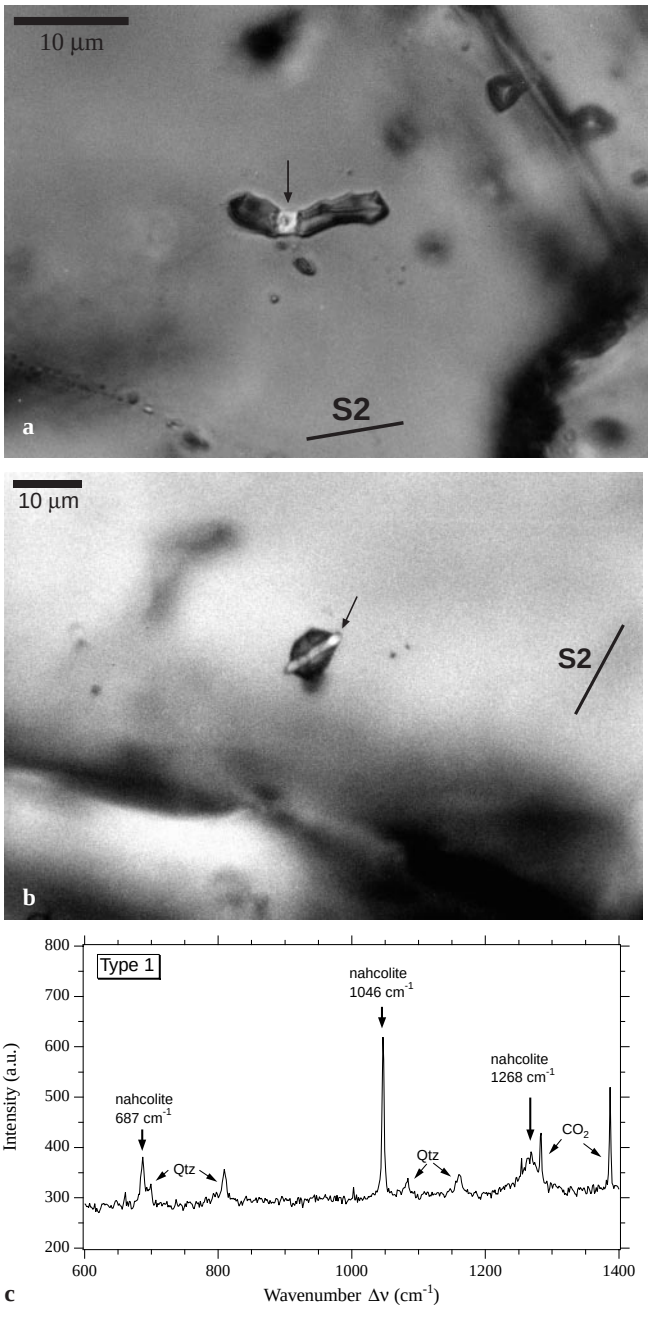

Fig. 5 **a** and **b** Photomicrographs of the occurrence of birefringent nahcolite in only part of type 1 fluid inclusion. The size of the nahcolite crystal in **b** clearly exceeds the size of the inclusion. **c** Raman spectrum of a nahcolite crystal (peaks at 687, 1046 and 1268 cm^{-1}) as observed in type 1 fluid inclusions

Type 5 fluid inclusions

This class comprises highly irregular and flat H_2O-rich fluid inclusions. They occur along straight flat lying trails which sometimes cut through grain boundaries of

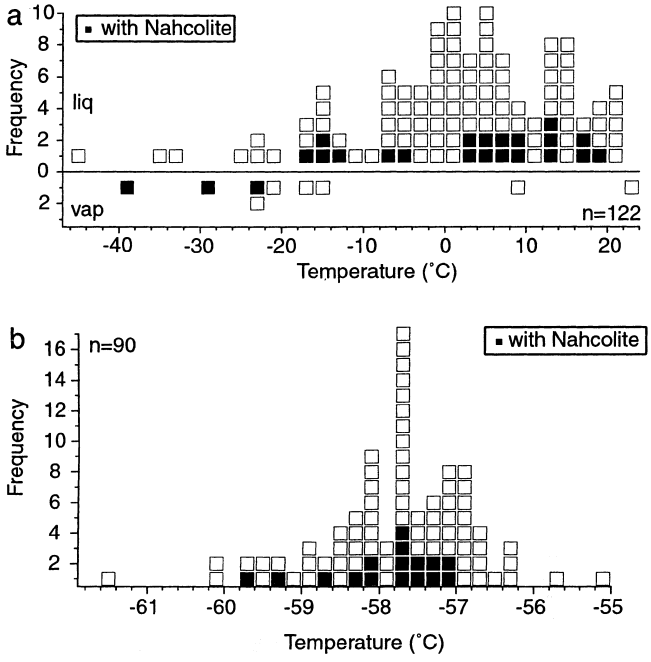

Fig. 6 Frequency distributions of homogenisation temperatures (**a**) and melting temperatures of the CO_2-rich phase (**b**) for type 1 fluid inclusions. Homogenisation occurs mostly in the liquid phase (*upper part* in **a**), some in the vapour phase (*lower part* in **a**). The *dark squares* illustrate those inclusions that contain a nahcolite crystal of variable size and volume percentage

quartz crystals. Filling degree is variable and in general >80 volume%. Melting temperature of ice around −0.3 °C indicates the nearly pure H_2O nature of this fluid. They are interpreted as a late generation of fluid inclusions.

Discussion

Bulk composition and molar volume calculations

A combination of homogenisation temperatures and Raman analysis of type 1 carbonic fluid inclusions allows an exact calculation of molar volumes (Table 4) using the computer program package *FLUIDS* (Bakker 1999). The modifications according to Thiéry et al. (1994) on the equation of state from Soave (1972) accurately represent experimental *P-T-x* solvus data of the CO_2-CH_4-N_2 fluid system and are, therefore, applied to type 1 fluid inclusions. Volumetric properties at these solvus conditions are calculated with the Lee and Kesler (1975) equation of state. In absence of Raman analysis, a graphical method was used to estimate bulk V-*X* fluid properties (e.g. Shepherd et al. 1985, pp. 113–120), using the V*X* diagrams for the binary systems CO_2-CH_4 and CO_2-N_2 from Thiéry et al. (1994). For this procedure it was assumed that the depression of the CO_2 melting temperature is caused by only one other gas species, either CH_4 or N_2. The calculated bulk molar volume and composition inferred from Table 1 vary between 44–70 cm^3/mole and 83–100 mol% CO_2, respectively.

Bulk molar volumes for type 3 fluid inclusions depend on estimation of volume fractions of the fluid phases. The complexity of the fluid system, i.e. mixtures of several gases (CO_2-CH_4-N_2), H_2O and salt prevents a direct transformation of total homogenisation temperatures into bulk densities. These fluid systems are not yet accurately investigated by experimental studies, consequently, data on solvus *PVTX* properties are not available. Therefore, volume fraction estimates are the most accurate approximations for these fluid systems. The aqueous fluid inclusions (group A) of type 3 have molar volumes between 18.3 and 30.1 cm^3/mole, with the assumption that the vapour bubble contains a low density gas phase. The molar volume of carbonic fluid inclusions (group C) of type 3 varies between 73 and 118 cm^3/mole. Assuming that the vapour bubble contains mainly CO_2 and that the salinity of the aqueous phase can be neglected, the CO_2 mole fraction has been calculated between approximately 0.23 and 0.37. These numbers are not seriously affected if CH_4 is a major constituent of the carbonic fluid instead of CO_2. Clathrate temperatures of the intermediate group B can only be transformed into specific densities if the salinity of the aqueous phase after clathrate melting is assumed to have an average value, which is similar to group A. For example, fluid inclusion 31 (Tables 3 and 4), which occupies approximately 40 volume%, contains 86 mol% CO_2 and 14 mol% CH_4 in the carbonic phase. The final clathrate melting temperature is +9.8 °C. Assuming a salinity of 5 wt% NaCl, the bulk molar volume and composition has been calculated at 29 cm^3/mole and 89 mol% H_2O, 7 mol% CO_2, and 1 mol% CH_4.

Isochore calculation

Using the data from Table 1 for type 1 fluid inclusions, isochores were calculated (Fig. 10) with the aid of computer program package *FLUIDS* (Bakker 1999). The isochores are calculated using the equation of state according to Duan et al. (1992, 1996) for mixtures of CO_2, CH_4, and N_2, which accurately reproduces experimental data of this fluid system at higher temperatures and pressures. The compressibility and expansion of the host mineral quartz (Hosieni et al. 1985) is taken into account in these calculations. These processes slightly adjust the density of the entrapped fluids during heating or cooling of the system and, consequently, they shift the fluid *PT* trajectory to different true isochoric lines. The estimated pressures at higher temperatures with uncorrected isochores may have been underestimated by a maximum of 70 MPa (Fig. 11). The isochore for inclusion number R38, which has the highest density, i.e. the minimum molar volume of 41.5 cc/mole shows the highest *PT* conditions amongst the measured inclusions. This isochore nearly coincides with the *PT* conditions of the rim of garnet porphyroblasts, determined independently with the aid of thermobarometric studies

Table 1 Microthermometrical data of carbonic (*car*) type 1 fluid inclusions: nucleation- (*Tn*), melting- (*Tm*) and homogenisation temperatures (*Th*), always into the liquid phase, unless indicated with *vap*. Temperatures are given in °C. Additionally, the presence of nahcolite (*Na*), approximate morphology and size (average diameter) are indicated

Inclusion no.	*Tn*	*Tm* (car)	*Th* (car)	*Na*	Morphology	Size (μm)
7	−93	−57.1	20.3		Negative crystal	11.5
8a	−99.3	−56.9	20		Rectangular	7.4
8b	−99.3	−56.9	20		Cubical	4.4
8c	−99.3	−56.9	20		Cylindrical	4.0
8d	−99.3	−56.8	21.6		Negative crystal	6.4
16	−96.3	−55.1	15.8		Spherical	4.4
17	−96.1	−56.7	18.3		Spherical	6.1
20	−100	−56.8	8.9		Cylindrical	3.7
R1a	−89.4	−57	3.4		Cylindrical	5.1
R1b	−89.4	−57	6.5		Cubical	4.7
R1c	−93.0		8.1		Spherical	3.0
R2	−93.0	−58.4	4.1		Negative crystal	2.0
R3a	−93.0	−57.7	12.3	+	Negative crystal	4.4
R3b			15.2		Spherical	3.0
R4a		−57.3	5.0		Spherical	2.7
R4b	−91.2	−57.3	5.6	+	Irregular	5.1
R4c			−2.3		Spherical	3.4
R4d		−56.9	−1.7		Cylindrical	4.4
R5a	−91.2	−56.8	−2.8		Spherical	5.4
R5b	−89.4	−56.7	0.9		Cylindrical	4.4
R5c	−93.0	−57.6	1.0		Negative crystal	5.7
R6a	−93.0	−58.2	4.6		Negative crystal	4.7
R6b	−92.1	−57.7	0.3		Cylindrical	6.1
R6c	−93.0	−57.7	7		Negative crystal	4.0
R11a	−92.1	−57	−0.9		Negative crystal	3.7
R11b			4.3		Spherical	
R18		−58.9	−9.1		Spherical	4.4
R21a		−57.9	0.1		Irregular cylindrical	
R21b			4.2		Cylindrical	
R22a	−98.1	−59.3	−16.2		Irregular spherical	5.7
R22b			2.4		Cylindrical	
R22c		−58.0	3.2		Negative crystal	
R23		−59.4	−15		Cubical	4.7
R24	−97.1	−58.2	−0.3		Irregular cylindrical	4.7
R25		−58.9	−10.2		Negative crystal	4.0
R26		−59.1	−15		Cubical	4.0
R27	−95.2	−57.5	12.5		Cylindrical	4.7
R28		−57.7	13.8	+	Cylindrical	3.0
R29					Rectangular	
R33		−57.2	−1.9		Negative crystal	5.1
R34		−57.7	−6.2		Negative crystal	6.7
R35		−57.6	0.3		Spherical	4.4
R36		−57.9	−22.4		Rectangular	4.0
R37 (=32)	−95.2	−57.6	−24.3		Cylindrical	3.7
R38 (=33)	−97.1	−57.7	−35.4		Negative crystal	4.0
R39 (=34)	−95.2	−57.6	−12		Spherical	3.0
R40 (=37)	−95.2	−57.5	−5.4	+	Cylindrical	5.4
R41 (=36)	−97.1	−57.9	−6.2		Spherical	2.7
R42		−57.4	−3.2		Spherical	3.0
R43 (=35)	−96.2	−57.6	−6.7	+	Cubical	5.7
R45		−59.3	8.1	+	Negative crystal	9.1
R46			15		Cubical	5.4
R47	−94.3	−57.6	17.3	+	Irregular cylindrical	14.2
R48		−57.7	14.7		Cylindrical	3.4
R49		−58.3	7.6		Irregular	4.7
R50		−58.3	2.0	+	Negative crystal	5.4
R51		−58.2	2.0		Negative crystal	6.4
R52	−100.2	−59.4	6.3		Irregular cylindrical	5.1
R53a			9.5	+	Spherical	4.1
R53b			10.4		Negative crystal	4.0
R54a		−58.9	10.6		Cylindrical	4.4
R54b		−58.5	10.5		Cubical	6.1
R55		−60.1(?)	3.6		Irregular cylindrical	6.1
R56		−58.1	17.3	+	Negative crystal	3.7
R57a	−97.3	−58.0			Negative crystal	3.7
R57b		−61.4	13.1		Spherical	4.7

Table 1 (*Cont.*)

Inclusion no.	*Tn*	*Tm* (car)	*Th* (car)	*Na*	Morphology	Size (μm)
R71a		−56.2	6.5		Negative crystal	4.4
R71b			−23.2		Cylindrical	
R72			13.0		Cylindrical	
R74		−57	12.3	+	Negative crystal	4.4
R75		−56.2	−1.3		Cylindrical	4.4
R76		−57.2	−1.8		Negative crystal	3.4
R77		−57.7	5.9		Rectangular	5.1
R78		−57.7	5.4		Spherical	
R88		−57.2	4.4	+	Spherical	3.4
R89		−56.4	−0.8		Negative crystal	3.7
R90		−56.9	1.1		Cylindrical	5.7
R91		−57.4	4.8	+	Negative crystal	4.4
R92		−57	7.0	+	Negative crystal	4.4
R94		−57	0.4		Spherical	4.4
R95a		−56.2	−2.6		Negative crystal	6.0
R95b			−1.1		Spherical	
R95c			1.2		Cylindrical	
R96		−57.7	4.3		Cylindrical	5.1
R97			13.5		Cylindrical	
R100			−7.5		Cubical	2.6
R101			0.8		Spherical	2.5
R102			−3.8		Negative crystal	3.3
R103			−13.7	+	Cylindrical	6.6
R104			6.9	+	Irregular cylindrical	7.8
R105			−16.7		Negative crystal	2.6
R106			−6.3		Irregular cylindrical	6.2
R107			−7.7		Negative crystal	2.0
R108			−1.1		Cubical	2.1
R109			−21.6		Spherical	3.0
R110			−33.8		Cylindrical	3.9
R111			0.2		Cylindrical	2.6
R112			−45.9		Irregular spherical	3.3
R113			−15.8		Cylindrical	2.0
R14	−98.1	−58.5	−23.4 (vap)		Negative crystal	5.7
R15		−58.6	−29.2 (vap)	+	Irregular cylindrical	
R16		−58.4	−21.9 (vap)		Irregular spherical	
R17		−59.6	−38.9 (vap)	+	Cubical	
R19	−99	−60	−14.9 (vap)		Negative crystal	
R20a		−59.6	−16.6 (vap)		Cylindrical	
R20b			−23.4 (vap)	+	Irregular spherical	4.0
R86		−57.4	8.8 (vap)		Cylindrical	
R114			22.8 (vap)		Irregular spherical	5.9
M1	−105	−58.6			Spherical	4.7
M2	−102	−58.1	19.4		Cylindrical	7.4
M3	−102	−58.1	19.4	+	Cylindrical	4.7
M4	−98	−55.7	19.4		Spherical	9.5
M5	−103	−58.0	17.4		Spherical	6.1
M6	−103	−58.1	15.4		Spherical	2.7
M7	−103	−58.1	15.4		Spherical	2.7
M8	−100	−56.6	14.1		Spherical	
M9	−101	−57.6	15.4		Cylindrical	8.8
M10	−101.5	−58.0			Cylindrical	

(Mamtani 1998; Mamtani et al. 1999a). Consequently, these fluids might have been trapped at *PT* conditions during growth of the rim of garnets. The isochores for other type 1 inclusions with lower density naturally pass through lower pressure conditions, which may illustrate entrapment of an evolving fluid during decompression.

Due to visual restrictions on the optical observation of fluid inclusions, a rim of water wetting the inclusion walls may be invisible. It is generally assumed that a maximum of 10 volume% of water can be overlooked in equidimensional fluid inclusions. Although H_2O was not detected by Raman spectroscopy, and none of type 1 inclusions reveals optically the presence of a water rim, a hypothetical isochore has been calculated to estimate the shift in isochore position due to the addition of 10 volume% H_2O. Fluid inclusion R38 contains 95 mol% CO_2 and 5 mol% N_2 (see Table 4). Addition of 10 volume% H_2O changes the bulk composition into 18.7 mol% H_2O, 77.2 mol% CO_2 and 4.1 mol% N_2. The bulk molar volume has decreased from 41.5 to

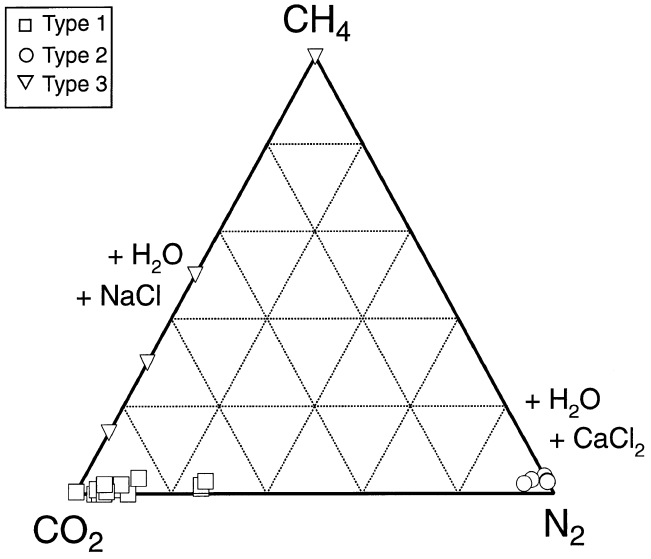

Fig. 7 CO_2-CH_4-N_2 compositional diagram for type 1, 2, and 3 fluid inclusions

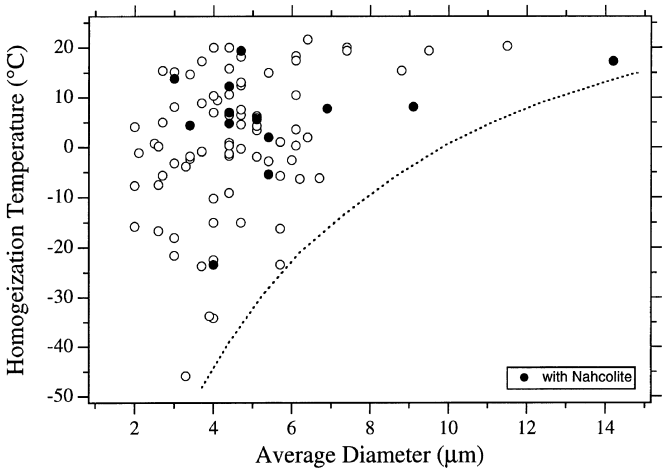

Fig. 8 Homogenisation-size diagram for type 1 fluid inclusions. The *dashed line* marks the apparent limit of observation, indicating the absence of large inclusions with high densities

36.7 cm^3/mole. The corrected isochore is now plotted between the garnet rim and core conditions (Fig. 11). Garnet-core *PT* conditions are reached if 20 volume% H_2O is assumed to be present in these inclusions; however, this amount of H_2O should be noticed in any kind of fluid inclusion. These hypothetical cases illustrate that the fluids in type 1 inclusions may well belong to the metamorphic *PT* conditions of growth of garnet porphyroblasts. However, the actual measured fluid properties indicate that fluids included during an earlier and higher-grade metamorphic event, as evidenced from the garnet-core mineralogy and relicts of high pressure quartz polymorphs, are not preserved.

Origin and timing of fluids

The high density CO_2-rich fluids in type 1 inclusions occur as isolated clusters in quartz. These clusters can be labelled "primary", and they are cut at a few places by inclusion trails belonging to type 2 and 3. These trails do not cross-cut any grain- or sub-grain-boundary. The presence of higher percentages of CH_4 in these inclusions may indicate a natural evolution of the circulating fluid in equilibrium with the mineral assemblage in the rocks during exhumation. Type 1 fluid inclusions represent the high temperature oxidised CO_2-rich fluids, and type 3 fluid inclusions illustrate a transition to lower temperature reduced CH_4-rich fluids. Although the position of N_2-rich fluids in type 2 is uncertain within this trend, cross-cutting relations of the inclusion trails suggest an intermediate origin, which may quantify the nitrodation state of the rock after garnet-rim metamorphic conditions. Mineral equilibria may define oxygen fugacities which influence directly the composition of fluids (e.g. Holloway 1977). French (1966) and Eugster and Skippen (1967) developed the calculation method for fluids in the C-O-H system, and compared fluid composition in equilibrium with several mineral buffers. Bakker and Jansen (1993) used a similar calculation method for the fluid evolution in the C-O-H-N system. In this study, N_2-rich fluids were obtained from a hy-

Table 2 Microthermometrical data of type 2 fluid inclusions: nucleation- (*Tn*), melting- (*Tm*), and eutectic temperatures (*Te*) of the aqueous phase (*aq*). Homogenisation temperature (*Th*) of the carbonic phase (*car*) is only observed in one inclusion. Temperatures are given in °C. Additionally, the volume% of the gas bubble and the approximate morphology are given

Inclusion no.	*T*h (car)	*T*n (aq)	*T*e	*T*m (aq)	Vol.% (gas)	Morphology
3		−58	−50.3	−14	5	Cylindrical
9		−70.6		−20.7	5	Cylindrical
11		−57.4		−19.8	20	Cylindrical
13		−68.6		−23.4	10	Cylindrical
R79a	−148 (vap)				90	Irregular spherical
R79b				−9.3	25	Cylindrical
R80		−78.2		−18.4	15	Negative crystal
R81		−76.3		−18.8	10	Cubical
R98		−53.3	−46.6 to −44.7	−17.2	20	Irregular cylindrical
M11				−19.8		Spherical

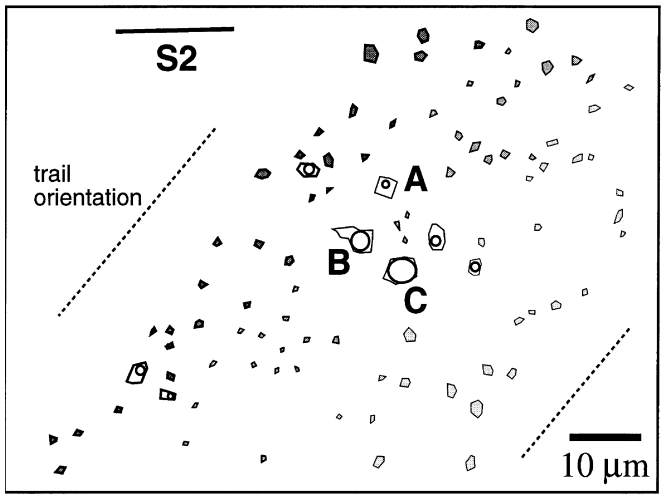

Fig. 9 A schematical drawing of type 3 fluid inclusions. Inclusions *A* and *C* represent the coexisting H_2O-rich liquid phase and gas-rich vapour phase, respectively, while inclusion *B* contains an intermediate type of fluid. The trail orientation is inclined to S2 and to the projection plane of view

pothetical mineral buffer at higher temperatures due to the lack of knowledge on the occurrence of nitrogen in natural minerals at metamorphic conditions. Although the activity of mineral assemblages buffering fluid compositions during the uplift path is uncertain in the schist studied, the oxidation states of the rock are generally compared to hypothetical mineral reactions including oxygen, for example, the QFM buffer (i.e. quartz-fayalite-magnetite). In other words, the oxidation state of a rock may be described by a buffer reaction, whose components are not necessarily present in the rock. Calculated trends in fluid evolution generally illustrate an oxidised CO_2-rich fluid at relatively high temperatures and a reduced CH_4-rich fluid at low temperatures, similar to the studied sample, while at intermediate temperatures H_2O appears to be a major constituent of the fluid with equal minor amounts of CO_2 and CH_4 (e.g. Fig. 3 in Holloway 1977).

Fluid conditions in granulite-facies rock have been inferred from fluid inclusions and mineral equilibria involving a fluid phase of either H_2O or CO_2 (e.g. Touret 1985; Lamb and Valley 1988). Calculations of fluids

Table 3 Microthermometrical data of type 3 fluid inclusions: nucleation- (*Tn*), melting- (*Tm*), eutectic- (*Te*) and homogenisation temperatures (*Th*). Melting of the carbonic phase (*car*), aqueous solution (*aq*), and clathrate phase (*clath*) are indicated. Temperatures are given in °C. Additionally, the volume% of the gas bubble and the approximate morphology are given. The groups are illustrative for heterogenic trapping, with intermediate types of fluid inclusions

Group	Inclusion no.	*Tn*	*Tm* (car)	*Th* (car)	*Te*	*Tm* (aq)	*Tm* (clath)	Vol.% (gas)	Morphology
A.	12	−45.3				−2.3		1	Cylindrical
	15	−53.2			< −8	−5.6		5	Cylindrical
	24	−53.4				−4.6		7	Spherical
	30	−49.3				−5.8		1	Irregular
	R8c					−4.9		20	Cylindrical
	R31	−44.7				−4.2		15	Cubical
	R58 (=26)	−47.5			−25 to −20	−4.3		7	Cubical
	R62	−49.5				−5.3		20	Rectangular
	R63					−2.8		40	Spherical
	R64					−3.8		30	Cubical
	R65					−6.1		20	Cylindrical
	R93	−49.5				−3.0		5	Spherical
B.	14	−50.3			−21.2		7.6	2	Cylindrical
	21	−30.9					8.7	30	Cylindrical
	22	−31.1					8.7	30	Cylindrical
	23	−31.5					7.8	30	Spherical
	25	−32.1					7.8	30	Cylindrical
	28	−38.9					8.8	30	Cubical
	29	−30.6					8.7	50	Cylindrical
	31	−29.7					9.8	40	Irregular
	R12						7.4	60	Cylindrical
	R59 (=27)	−36.7					6.8	40	Irregular
	M13	−35.8					10.2	40	Cylindrical
	M14	−39					7.3	20	Spherical
	M15	−37.5					8.4	20	Spherical
	M16						7.4	40	Spherical
	M17	−37.5					8.0	30	Spherical
	M18	−36.5					9.2	30	Spherical
C.	R8a	−93 (car)	−57.1	14.6 (vap)				80	Cylindrical
	R8b	−93 (car)	−56.7	12.7 (vap)				90	Cylindrical
	R13	−100.9 (car) −34 (ice)	−61.2	18.2 (liq)			5.5	30	Spherical
	R60	−95.2 (car)	−56.3				7.6	90	Irregular spherical
	R61	−95.5 (car)							Irregular spherical
	R84		−57.3						Cubical

Table 4 Results of Raman microprobe spectroscopy for some type 1, 2 and 3 fluid inclusions, in addition to microthermometry: melting temperature (*Tm*) and homogenisation temperature (*Th*) of the carbonic phase (*car*). V_M is the calculated molar volume

Inclusion type	Inclusion no.	*Tm* (car) (°C)	*Th* (car) (°C)	Composition carbonic phase (mol%)			V_M (cc/mole)
				CO_2	CH_4	N_2	
1	7	−57.1	20.3 (liq)	90	1 ± 0.3	9 ± 2	89.9 ± 12.0
	8a	−56.9	20.0 (liq)	95	1 ± 0.3	4 ± 1	63.3 ± 3.1
	A	–	–	89	–	11 ± 2	–
	R37(32)	−57.6	−24.3 (liq)	96	–	4 ± 1	43.13 ± 0.08
	R38(33)	−57.7	−35.4 (liq)	95	–	5 ± 1	41.52 ± 0.02
	R40(37)	−57.5	−5.4 (liq)	95	1 ± 0.3	4 ± 1	48.31 ± 0.30
	R40[a]			94[a]	–	6 ± 2[a]	48.04 ± 0.03
	R43(35)	−57.6	−6.7 (liq)	93	2 ± 0.5	5 ± 1	48.22 ± 0.03
	R43[a]			94[a]	–	6 ± 2[a]	47.65 ± 0.05
	R95	−56.2	−2.6 (liq)	99.5	0.5 ± 0.2	–	46.91 ± 0.16
	MU2	–	–	89.4	2.1 ± 0.5	8.5 ± 2	–
	MU3	–	–	93.2	0.5 ± 0.1	6.3 ± 1	–
	MU8	–	–	92.8	2.2 ± 0.5	5 ± 1	–
	MU9	–	–	73.1	1.3 ± 0.3	25.6	–
	MU10	–	–	72.8	1.9 ± 0.5	25.3	–
	MU15	–	–	85	3.6 ± 0.9	11.4 ± 2	–
	MU18	–	–	71.4	2.9 ± 0.7	25.7	–
2	39	–	–	–	3 ± 1	97	–
	R79	–	−148 (vap)	–	4 ± 1	96	–
	D	–	–	–	–	100	–
	MU1	–	–	–	2.8 ± 0.7	97.2	–
	MU5	–	–	–	2.9 ± 0.7	97.1	–
	MU11(R79)[a]	–	–	3.1 ± 0.8[a]	3.2 ± 0.8[a]	93.7[a]	–
	MU12			5.1 ± 1	2.3 ± 0.6	92.6	
	MU16	–	–	–	2.7 ± 0.7	97.3	–
3	C	–	–	70	30 ± 4	–	–
	R59(27)	–	–	50	50 ± 12	–	–
	40	–	–	–	100	–	–
	31	–	–	86	14 ± 3	–	–
	MU7	–	–	–	100	–	–

[a] Duplicate measurements, within a time span of 2 months

buffered by mineral assemblages resulted in a wide variety of possible fluid compositions, dependent on the chosen active equilibrium in specific samples and uncertainties from adequate calibrated thermodynamic properties of mineral equilibria. This calculated fluid is in general H_2O-poor and either CO_2-rich or CH_4-rich from mineral equilibria involving H_2O, while other equilibria involving CO_2 in adjacent samples result in low CO_2 activities (e.g. Lamb and Valley 1988). In this study, the sensitivity of a calculated fluid composition to changes in oxygen fugacity at metamorphic conditions during garnet-rim growth, i.e. 775 K and 545 MPa, is illustrated in Fig. 12. Calculations in the C-O-H fluid system are performed with the computer program *FLEVOL* (Bakker 1992), specially designed for fluid calculations from defined mineral equilibria and selected temperature and pressure conditions. The presence of graphite in both matrix and type 1 fluid inclusions defines its activity at 1. Within an extremely short range of oxygen fugacities the composition of the fluid may change completely, e.g. from a CO_2-rich to a H_2O-rich fluid (Fig. 12). Consequently, a wide variety of fluid properties may be present in natural rock due to only small variations or fluctuations in the oxygen fugacity. At oxygen fugacities higher than $10^{-22.22}$ MPa the fluid system is over-determinated and only one buffer, either graphite or an oxygen buffer, may define the whole fluid system, consisting mainly of CO_2. Because an oxygen buffer is not defined from the studied rock and graphite is still present, it is proposed that CO_2-rich fluid inclusions from type 1 may correspond to a buffered fluid at metamorphic conditions during garnet-rim growth. These calculations do not include N_2 or any type of salt, which may seriously affect the fluid properties at metamorphic conditions.

The evidence for granulitic fluid conditions from fluid inclusions, which are in general CO_2-rich and have a relative high density, has been considered questionable because peak metamorphic conditions are not always reproduced by isochore tracing of inclusions that belong to the same generation. The scatter to lower densities has resulted from either re-equilibration of fluid inclusions that have all been trapped at peak metamorphic conditions, or a later stage entrapment, as preferred by Lamb et al. (1987). However, the presence of fluid densities that do represent peak metamorphic condition illustrates the ability of quartz to preserve original fluids, even from granulites.

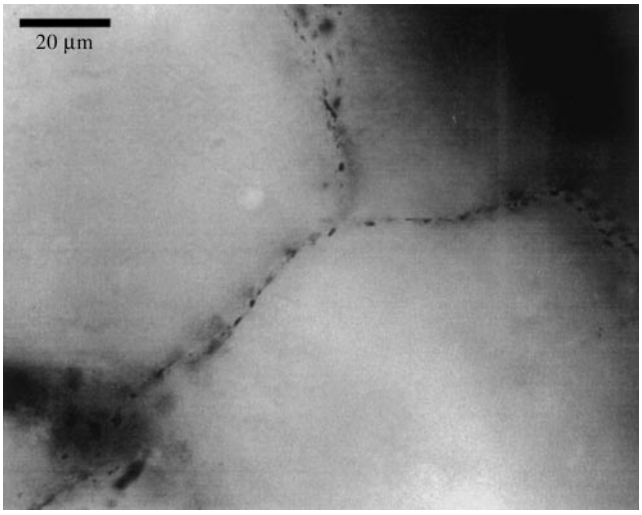

Fig. 10 Photomicrograph of fluid inclusions along grain boundaries, i.e. type 4 fluid inclusions

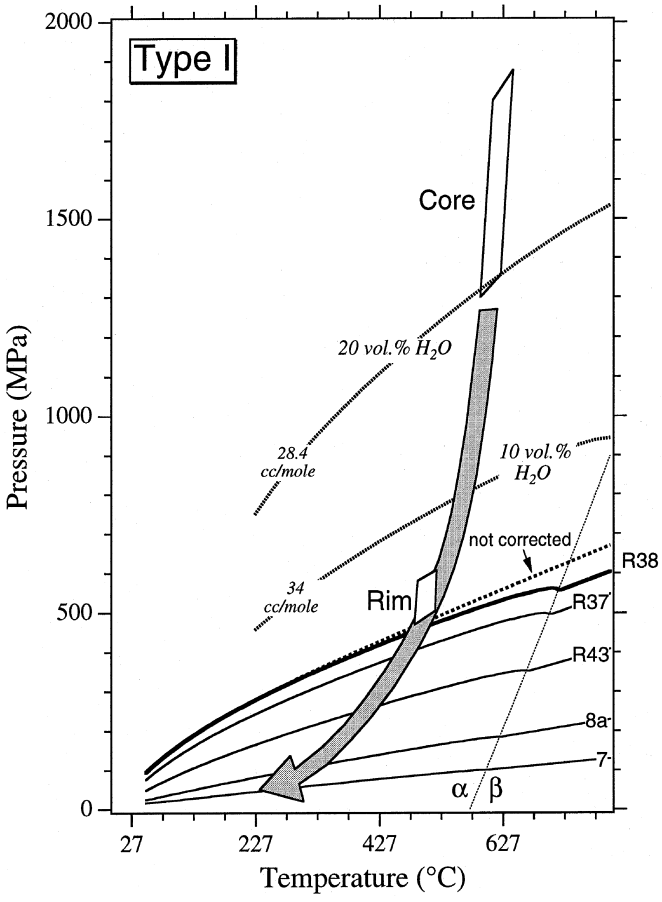

Fig. 11 *P-T* diagram with calculated conditions from geothermobarometers for the core of garnets (*Core*) and the rim of garnets (*Rim*). The alpha-beta transition of quartz is illustrated with a *dashed line*. Isochores are projected for some type 1 fluid inclusions as presented in Table 4. Isochores are corrected for host-mineral expansion and compressibility, and the corresponding shift is illustrated for inclusion R38. Two hypothetical amounts of H_2O, i.e. 10 vol.% and 20 vol.%, for inclusion R38 are indicated by *two dashed isochores*. Their *numbers* represent the calculated molar volumes

Types 2 and 3 fluid inclusions show evidence of heterogeneous fluid trapping, which is a common process in any salt-bearing system because the fluid immiscibility extends to higher temperatures and pressures. It is envisaged that in type 2 inclusions, N_2 and $CaCl_2$ has been introduced in the fluid system from aqueous fluids supposedly from an external source, which could have been the Godhra granite intrusion. At equilibrium, immiscibility into a high density H_2O-salt-rich fluid and a low density gas-rich fluid must have occurred relatively quickly, and thus remained preserved in the fluid inclusions. This process is in accordance to the theoretical considerations from Rice and Ferry (1982) who mentioned that the local bulk fluid composition may be controlled by local thermodynamic conditions, even after infiltration of an external fluid. During the formation of type 3 inclusions, a completely different type of fluid must have intruded the system, carrying NaCl-rich aqueous fluids with a much lower salinity. Timing of type 4 fluid inclusions in relation to types 1, 2 and 3 is more uncertain, because the inclusions were too small for microthermometrical analysis. On the basis of crystal size distribution (CSD) studies of quartz crystals in the schist presently investigated, Mamtani and Karanth (1996) have shown that the quartz crystals underwent considerable annealing. This was correlated with heat supplied by the Godhra granite, which intruded the rocks. Therefore, type 4 fluid inclusions are considered to have formed during recrystallisation and annealing of quartz crystals, due to heat supplied by this granite.

Re-equilibration processes

Decrepitation, i.e. non-elastic deformation of crystals around fluid inclusions, may result in complete loss of fluids if the induced cracks are connected to the pore spaces. Partial decrepitation results in an uncontrolled total volume increase, which must lead to fluid density decrease if the total amount of fluid is not lost from the system. Experimental studies by Leroy (1979) and Bodnar et al. (1989) give a rough relation between inclusion size and decrepitation behaviour at 1 atmosphere confining pressure. Swanenberg (1980) observed this size effect in natural monophase carbonic inclusions in rocks from Faurefjell metasediments in high-grade metamorphic Precambrians of south-west Norway. He suggested that the relation between inclusion size and homogenisation temperature reflects the enhanced mechanical strength of smaller sized inclusions during the post-entrapment period. Relatively large inclusions are more likely to undergo decrepitation and subsequent leakage. It can be argued that there is a possibility of loss of fluid from type 1 inclusions due to overpressure as the rocks were uplifted to the Earth's surface. Figure 8 shows the relationship between average diameter of type 1 fluid inclusions and homogenisation temperatures. Large in-

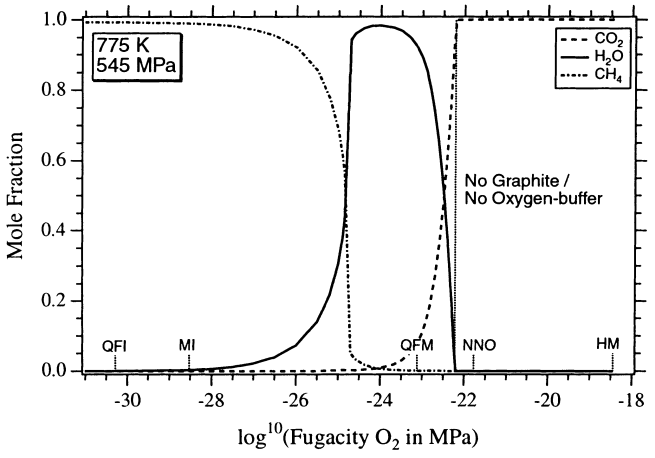

Fig. 12 Mole fractions of CO_2, H_2O and CH_4 calculated as a function of oxygen fugacity in the presence of graphite at 775 K and 545 MPa. Several standard oxygen buffers are illustrated: (*QFI* quartz-fayalite-iron, *MI* magnetite-iron, *QFM* quartz-fayalite-magnetite, *NNO* nickel-nickel oxide, *HM* hematite-magnetite). The equation of state from Holloway (1977) and Flowers (1979) are used to calculate fugacities of fluid species. Minor amounts of H_2 and CO are not revealed in the diagram

clusions with high densities appear to be absent, while smaller inclusions represent a broader temperature range, i.e. density range. It is assumed that during the formation of fluid inclusions all sizes are randomly distributed within grains. If the rock undergoes decompression during uplift, the fluid may evolve smoothly to lower densities, which will be recorded in newly formed fluid inclusions of all sizes. Consequently, fluid inclusions would be found having all sizes and densities, and no general trend would have been recognised in Fig. 8. However, the first formed inclusions have to endure an increasingly expanding internal overpressure, and only the larger inclusions will be lost by decrepitation processes, similar to the previously described experiments. The smaller inclusions can resist these overpressures, and remain conserved during further exhumation of the rock. These processes may lead to the observed trend in Fig. 8. In addition to these brittle phenomena, ductile deformation of the inclusion walls may have been the most important process producing increased total volume of inclusions due to internal overpressures. Both types of deformation may lead to similar observations as illustrated in Fig. 8.

The appearance of nahcolite in only some of type 1 fluid inclusions (Fig. 5) has some implications on the nature of the fluid that was present during entrapment. The wide variation in volume ratios of nahcolite and carbonic fluid suggests that these crystals are accidentally trapped solids. Mainly those nahcolite crystals, which exceed the size of fluid inclusion, imply the presence of small crystals in the circulating fluid before complete sealing of the fluid inclusions. Nahcolite has been observed as a daughter mineral in fluid inclusions in rocks of magmatic origin, e.g. ijolite pegmatites and carbonatites (Rankin and Le Bas 1974; Aspen 1980; Walther 1981), and phonolites (Vard and William-Jones 1993). Andersen et al. (1989) and Samson et al. (1997) report nahcolite daughter minerals in fluid inclusions in high-grade metamorphic rocks like eclogites and greenstone belts, respectively, wherein the origin of these nahcolite-bearing fluids is believed to be magmatic, e.g. alkaline carbonatite magmatism and lamprophyre dikes. The nature of these fluids is a concentrated, highly alkaline aqueous solution with a high HCO_3^- content, or an excess of CO_2. Olsen (1987) has described nahcolite crystals in nearly pure CO_2 fluid inclusions in migmatites, similar to the occurrence in type 1 fluid inclusions, and suggested that those inclusions must have contained some H_2O in the past. The presence of nahcolite does not necessarily indicate initial major amounts of water in the fluid inclusions studied. Two immiscible fluid phases, i.e. a brine and a carbonic fluid, both saturated with respect to nahcolite, may have been present in the pore space, and either preferential trapping of the carbonic fluid, or loss of brine inclusions by later processes (Andersen et al. 1991) caused the preservation of only one fluid type. If both fluids became super-saturated with respect to nahcolite before the inclusions were completely sealed, accidentally trapped crystals may occur in type 1 fluid inclusions. However, the studied sample has no traces of heterogeneous trapping during the formation of type 1 fluid inclusions, whereas traces of this process are preserved for type 3 fluid inclusions. The amount of nahcolite present in the carbonic inclusions exceeds any estimation from super-saturated solutions, because nahcolite would mainly be concentrated in the brine. Furthermore, nahcolite crystals would be expected to be present as solid inclusions in quartz, as relicts from the super-saturated brine-like fluid, however, these crystals were only observed in type 1 fluid inclusions.

Therefore, the presence of nahcolite in type 1 fluid inclusions in the schist sample presently investigated may indicate the aqueous nature of the original fluid that was present during entrapment. The aqueous character of this fluid is completely lost during the metamorphic evolution of the rock after entrapment of type 1 fluid inclusions. Preferential H_2O-leakage from fluid inclusions, as described by Bakker and Jansen (1991, 1994) during decompression of the rock, must have occurred within these inclusions, leaving a nearly pure high density carbonic fluid. Ductile deformation of the inclusion walls at high temperature and pressure resulted in extensive straining of the quartz and introduced a high density of dislocations in near vicinity of the inclusions, which subsequently could have preferentially extracted H_2O from the inclusions. This phenomena enhanced deformation processes and stimulated compositional changes of the primary type 1 inclusion. Moreover, this lost water may have been redistributed in newly formed small bubbles along dislocation lines. This complex post-entrapment fluid

immiscibility process has been experimentally studied by Bakker and Jansen (1994), and appears to be effective in some synthetic fluid inclusions in natural quartz. Optical evidence of these deformation structures in the samples may have been completely obliterated during the previously described late stage recrystallisation.

Concluding remarks

A biotite-garnet schist from the Southern Aravalli Mountain Belt (NW India) reveals the presence of at least five generations of fluid inclusions in quartz crystals, which are carefully classified according to morphology and distribution in combination with microthermometric measurements and Raman spectroscopy. Relicts of the original peak metamorphic fluid. i.e. high density CO_2-N_2-rich fluids, are found in the relatively oldest type of inclusions, which occur as isolated clusters in quartz crystals. Although these inclusions reveal a large range in density, isochoric calculations for the highest density inclusions verify the independently obtained *PT* condition from garnet-biotite geothermobarometry. The actual measured fluid properties indicate that fluids included during an earlier and higher-grade metamorphic event, as evidenced from the garnet-core mineralogy and relicts of high pressure quartz polymorphs, are not preserved.

The fluid may well have been buffered by graphite during metamorphism, as it has been identified by Raman spectroscopy in both fluid and solid inclusions, whereas the mineralogy does not allow the use of any other mineral buffer for fluid property calculations. Calculated fluid composition corresponds to a CO_2-rich fluid at metamorphic conditions during growth of the garnet rim. However, these calculations may result in a wide variety of possible fluid compositions, depending on the chosen active equilibrium in specific samples and uncertainties from adequate calibrated thermodynamic properties of mineral equilibria. Moreover, these calculations do not include the presence of any salt, which seriously influences the properties of fluids by introducing a large immiscibility field.

Re-equilibration processes during a nearly isothermal uplift are manifested by a specific size-density distribution, and the occurrence of nahcolite as an accidentally trapped mineral in some high density water-free carbonic fluid inclusions. The absence of an aqueous phase may be evidence of the preferential leakage of H_2O from these inclusions. The source of a nahcolite-bearing fluid is unknown.

Heterogeneous trapping is evidence for the second and third type of fluid inclusions. Healed fractures with specific orientation for both types were responsible for refilling some intersected primary inclusions with N_2-rich fluids (second type) and CO_2-CH_4 (third type). A coexisting high saline $CaCl_2$-rich aqueous fluid (up to 23.3 eq.wt% $CaCl_2$) occurs in small inclusions belonging to the second type, while the third type consist of a low saline NaCl-bearing aqueous solution (up to 8.9 eq.wt% NaCl).

The last two types of inclusions represent grain boundary fluids and a nearly pure H_2O-rich fluid, respectively, typically generated during a late stage of the uplift history.

Acknowledgements Fieldwork and sample collection for the present study was done when M.A.M. was holder of a Council of Scientific and Industrial Research (CSIR, New Delhi) Senior Research Fellowship (No. 9/114/(92)/96/EMR-I). Fluid inclusion studies and research at Geologisch-Paläontologisches Institut, University of Heidelberg (Germany) were possible through a German Academic Exchange Service Fellowship (No. A/97/00792) awarded to M.A.M. by the DAAD, Bonn (Germany). R.O. Greiling (Heidelberg), R.V. Karanth (Vadodara, India) and S.S. Merh (Vadodara) are thanked for encouragement and discussions. J. Touret and T. Andersen are greatly thanked for reviewing this manuscript. The authors are grateful to E.A.J. Burke for carrying out Raman microspectrometric analysis at the Free University, Amsterdam (The Netherlands). Thanks are also due to Rainer Altherr, Hans P. Meyer and Gültekin Topuz for extending all facilities and help to make microprobe measurements at the Mineralogisches Institut (Heidelberg).

References

Andersen T, Burke EAJ, Austrheim H (1989) Nitrogen-bearing, aqueous fluid inclusions in some eclogites from the Western Gneiss Region of the Norwegian Caledonides. Contrib Mineral Petrol 103: 153–165

Andersen T, Austrheim H, Burke EAJ (1991) Mineral-fluid-melt interactions in high-pressure shear zones in the Bergen Arc nappe complex, Caledonides of W. Norway; implications for the fluid regime in Caledonian eclogite-facies metamorphism. Lithos 27: 187–204

Aspen JA (1980) The mineralogy of primary inclusions in apatite crystals extracted from Alnö ijolite. Lithos 13: 263–268

Bakker RJ (1992) On modification of fluid inclusions in quartz: re-equilibration experiments and thermodynamic calculations on fluids in natural quartz. PhD thesis, Univ Utrecht, Geol Ultraiectina 94

Bakker RJ (1997) Clathrates: computer programs to calculate fluid inclusion V-*X* properties using clathrate melting temperatures. Comput Geosci 23: 1–18

Bakker RJ (1999) Optimal interpretation of microthermometrical data from fluid inclusions: thermodynamic modelling and computer programming. Habilitation thesis, Univ Heidelberg, Germany

Bakker RJ, Jansen JBH (1991) Experimental post-entrapment water loss from synthetic CO_2-H_2O inclusions in natural quartz. Geochim Cosmochim Acta 55: 2215–2230

Bakker RJ, Jansen JBH (1993) Calculated fluid evolution path versus fluid inclusion data in the COHN system as exemplified by metamorphic rock from Rogaland, south-west Norway. J Metamorphic Geol 11: 357–370

Bakker RJ, Jansen JBH (1994) A mechanism for preferential H_2O leakage from fluid inclusions in quartz, based on TEM observations. Contrib Mineral Petrol 116: 7–20

Bodnar RJ, Binns PR, Hall DL (1989) Synthetic fluid inclusions. VI. Quantitative evaluation of the decrepitation behaviour of fluid inclusions in quartz at one atmosphere confining pressure. J Metamorphic Geol 7: 229–242

Burke EAJ (1994) Raman microspectrometry of fluid inclusions: the daily practice. In: de Vivo B, Frezzotti ML (eds) Fluid inclusions in minerals: methods and applications. Short Course Int Mineral Assoc, pp 25–44

Burke EAJ, Lustenhouwer WJ (1987) The application of a multichannel laser Raman microprobe (Microdil-28®) to the analysis of fluid inclusions. Chem Geol 61: 11–17

Duan Z, Møller N, Weare JH (1992) An equation of state for the CH_4-CO_2-H_2O system. II. Mixtures from 50 to 1000 °C and 0 to 1000 bar. Geochim Cosmochim Acta 56: 2619–2631

Duan Z, Møller N, Weare JH (1996) A general equation of state for supercritical fluid mixtures and molecular dynamics simulation of mixture *PVTX* properties. Geochim Cosmochim Acta 60: 1209–1216

Duschek W, Kleinrahm R, Wagner W (1990) Measurement and correlation of the (pressure, density, temperature) relation of carbon dioxide. II. Saturated-liquid and saturated-vapour density and the vapour pressure along the entire coexistence curve. J Chem Thermodyn 22: 841–864

Eugster HP, Skippen GB (1967) Igneous and metamorphic reactions involving gas equilibria. In: Abelson PH (ed) Researches in geochemistry. J Wiley, London, pp 492–520

Flowers GC (1979) Correction of Holloway's (1977) adaptation of the modified Redlich-Kwong equation of state for calculation of the fugacities of molecular species in supercritical fluids of geological interest. Contrib Mineral Petrol 69: 315–318

French BM (1966) Some geological implications of equilibrium between graphite and a C-H-O gas phase at high temperatures and pressures. Rev Geophys 4: 223–253

Gopalan K, Trivedi JR, Merh SS, Patel PP, Patel SG (1979) Rb-Sr age of Godhra and related granites, Gujarat (India). Proc India Acad Sci Earth Planet Sci 88A: 7–17

Gopalan K, Macdougall JD, Roy AB, Murali AV (1990) Sm-Nd evidence for 3.3 Ga old rocks in Rajasthan, northwestern India. Precambrian Res 48: 287–297

Gupta SN, Arora YK, Mathur RK, Iqbaluddin, et al (1980) Lithostratigraphic map of Aravalli region, Southern Rajasthan and Northern Gujarat. Geol Surv India Publ, Hyderabad

Gupta SN, Mathur RK, Arora YK (1992) Lithostratigraphy of Proterozoic rocks of Rajasthan and Gujarat – a review. Rec Geol Surv India 115: 63–85

Heron AM (1953) The geology of central Rejputana. Mem Geol Surv India 79

Hollister LS (1990) Enrichment of CO_2 in fluid inclusions in quartz by removal of H_2O during crystal-plastic deformation. J Struct Geol 12: 895–901

Holloway JR (1977) Fugacity and activity of molecular species in supercritical fluids. In: Fraser DG (ed) Thermodynamics in geology. Reidel, Dordrecht, pp 161–182

Hosieni KR, Howald RA, Scanlon MW (1985) Thermodynamics of the lambda transition and the equation of state of quartz. Am Mineral 70: 782–793

Küster M, Stöckhert B (1997) Density changes of fluid inclusions in high-pressure low-temperature metamorphic rocks from Crete: a thermobarometric approach based on the creep strength of the host minerals. Lithos 41: 151–167

Lamb WM, Valley JW (1988) Granulite-facies amphibole and biotite equilibria, and calculated peak metamorphic water activities. Contrib Mineral Petrol 100: 349–360

Lamb WM, Valley JW, Brown PE (1987) Post-metamorphic CO_2-rich fluid inclusions in granulites. Contrib Mineral Petrol 96: 485–495

Lee BI, Kesler MG (1975) A generalised thermodynamic correlation based on three-parameter corresponding states. American Institute of Chemical Engineers Journal 21: 510–526

Leroy J (1979) Contribution à l'étalonnage de la pression interne des inclusions fluides lors de leur décrépitation. Bull Mineral 102: 584–593

Mamtani MA (1998) Deformational mechanisms of the Lunavada Pre-Cambrian rocks, Panchmahal district, Gujarat. PhD thesis, M.S. Univ Baroda, Vadodara, India

Mamtani MA, Karanth RV (1996) Effect of heat on crystal size distribution of quartz. Curr Sci 70: 396–399

Mamtani MA, Karanth RV (1997) Syntectonic growth of porphyroblasts over crenulation cleavages – an example from the Precambrian rocks of the Lunavada Group, Gujarat. J Geol Soc India 50: 171–178

Mamtani MA, Karanth RV, Greiling RO (1998) Regional scale superposed folding in the Precambrian rocks of the southern Aravalli mountain belt, India (abstract). Symp TSK-7, Freiberg Forschungsh C471: 141–142

Mamtani MA, Greiling RO, Karanth RV, Merh SS (1999a) Orogenic deformation and its relation with AMS fabric – an example from the southern Aravalli mountain belt, India. In: Radhakrishna T, Piper JD (eds) The Indian subcontinent and Gondwana: a palaeomagnetic and rock magnetic perspective. Geol Soc India Mem 44: 9–24

Mamtani MA, Karanth RV, Greiling RO, Merh SS (1999b) Uplift orogenesis – an example from Proterozoic rocks of the southern Aravalli mountain belt, India (abstract). Exhumation of metamorphic terranes – abstr vol, Univ Rennes: 51

Mamtani MA, Karanth RV, Merh SS, Greiling RO (2000). Tectonic evolution of the southern part of Aravalli mountain belt and its environs – possible causes and time constraints. Gondwana Research 3: 175–187

Olsen SN (1987) The composition and role of the fluid in migmatites: a fluid inclusion study of the Front Range rocks. Contrib Mineral Petrol 96: 104–120

Rankin AH, Le Bas MJ (1974) Nahcolite ($NaHCO_3$) in inclusions in apatites from some E. African ijolites and carbonatites. Mineral Mag 39: 564–570

Rice JM, Ferry JM (1982) Buffering, infiltration, and the control of intensive variables during metamorphism. In: Ferry JM (ed) Characterization of metamorphism through mineral equilibria. Rev Mineral 10: 207–262

Roy AB, Kröner A (1996) Single zircon evaporation ages constraining the growth of the Archean Aravalli craton, northwestern Indian shield. Geol Mag 133: 333–342

Samson IM, Bas B, Holm PE (1997) Hydrothermal evolution of auriferous shear zones, Wawa, Ontario. Econ Geol 92: 325–342

Shepherd TJ, Rankin AH, Alderton DHM (1985) A practical guide to fluid inclusion studies. Blackie, Glasgow and London

Soave G (1972) Equilibrium constants from a modified Redlich-Kwong equation of state. Chem Eng Sci 27: 1197–1203

Sorby HC (1858) On the microscopical structure of crystals, indicating the origin of minerals and rocks. J Geol Soc London 14: 453–500

Span R, Wagner W (1996) A new equation of state for carbon dioxide covering the fluid region from the triple-point temperature to 1100 K at pressures up to 800 MPa. J Phys Chem Ref Data 25: 1509–1596

Sterner SM, Bodnar RJ (1989) Synthetic fluid inclusions. VII. Re-equilibration of fluid inclusions in quartz during laboratory-simulated metamorphic burial and uplift. J Metamorphic Geol 7: 243–260

Swanenberg HEC (1980) Fluid inclusions in high-grade metamorphic rocks from S. W. Norway. PhD thesis, Geologica Ultraiectina 25, pp 147

Thiéry R, van den Kerkhof AM, Dubessy J (1994) V*X* properties of CH_4-CO_2 and CO_2-N_2 fluid inclusions: modelling for $T < 31$ °C and $P < 400$ bars. Eur J Mineral 6: 753–771

Tobisch OT, Collerson KD, Bhattacharya T, Mukhopadhyay DM (1994) Structural relationship and Sm-Nd isotopic systematics of polymetamorphic granite gneisses and granitic rocks from central Rajasthan, India: implication for evolution of the Aravalli craton. Precambrian Res 65: 319–339

Touret JLR (1977) The significance of fluid inclusions in metamorphic rocks. In: Fraser DG (ed) Thermodynamics in geology. Reidel, Dordrecht, pp 203–227

Touret JLR (1985) Fluid regime in Southern Norway: the record of fluid inclusions. In: Tobi AC, Touret JLR (eds) The deep

proterozoic crust in the North Atlantic Provinces, Reidel, Dordrecht, pp 517–549

Vard E, Williams-Jones AE (1993) A fluid inclusion study of vug minerals in dawsonite-altered phonolite sills, Montreal, Quebec: implications for HFSE mobility. Contrib Mineral Petrol 113: 410–423

Vityk MO, Bodnar RJ (1995) Textural evolution of synthetic fluid inclusions in quartz during reequilibration, with applications to tectonic reconstruction. Contrib Mineral Petrol 121: 309–323

Walther J (1981) Fluide Einschlüsse im Apatit des Carbonatits vom Kaiserstuhl (Oberrheingraben): ein Beitrag zur Interpretation der Carbonatitgenese. PhD thesis, Univ Karlsruhe, Germany